

Three-dimensional spatially resolved optical energy density enhanced by wavefront shaping: supplementary material

PEILONG HONG,^{1,2,*} OLUWAFEMI S. OJAMBATI,^{1,3,*} AD LAGENDIJK,¹ ALLARD P. MOSK,^{1,4} AND WILLEM L. VOS,^{1,**}

¹Complex Photonic Systems (COPS), MESA+ Institute for Nanotechnology, University of Twente, P.O. Box 217, 7500 AE Enschede, The Netherlands

²Present address: Faculty of Science, Ningbo University, Ningbo 315211, China

³Present address: NanoPhotonics Center, Cavendish Laboratory, University of Cambridge, United Kingdom

⁴Present address: Nanophotonics, Debye Institute, Utrecht University, P.O. Box 80.000, 3508 TA Utrecht, The Netherlands

*These authors contributed equally.

**Corresponding author: w.l.vos@utwente.nl

Published 12 July 2018

This document provides supplementary information to "Three-dimensional spatially resolved optical energy density enhanced by wavefront shaping," <https://doi.org/10.1364/OPTICA.5.000844>. We discuss the ZnO scattering samples, the optical wavefront shaping setup including the data acquisition times and wavefront shaping fidelity, and we elaborate on the 3D model for the enhanced energy density as a result of wavefront shaping.

1. SAMPLES

Our scattering samples are made of ZnO nanoparticles that are sparsely doped with fluorescent spheres. We first diluted the original aqueous suspension of fluorescent spheres (Thermo Scientific Fluoro-Max Red Aqueous Fluorescent Particles with concentration of 1%, radius $R = 150$ nm, fluorescence wavelength centered at $\lambda_f = 612$ nm) to 10^5 times, then added 2.5 g ZnO nanoparticles (Sigma-Aldrich Zinc Oxide 205532, average radius $R = 100$ nm) into 10 ml of the diluted suspension. We fabricated the samples by spraying the thoroughly mixed suspension on a cleaned objective substrate glass, and letting it dry in air. The thickness L of the sample was controlled by the spraying time.

To characterize the scattering properties of the samples, total transmission measurements were performed on similar samples to determine the transport mean free path to be $\ell = 0.58^{+0.16}_{-0.10}$ μm (see Ref. [1]).¹ We derive the extrapolation lengths from the average reflectivity at the interfaces for a scattering medium with effective refractive index n_{eff} [2]. The effective refractive index n_{eff} was determined from measurements of the angle-resolved

¹ The photonic interaction strength is about $1/(k\ell) = 1/(2\pi)$ (k is the wave vector), which is in the diffusive regime [14]. Moreover, since we consider the diffuse energy density, interference effects such as weak localization are averaged.

escape function on similar samples, to find $n_{\text{eff}} = 1.45 \pm 0.12$ and extrapolation lengths $z_{e1} = 2.19\ell$, $z_{e2} = 0.68\ell$ [1].

To ensure that the distribution of the energy density at λ_e inside the scattering medium is not perturbed by the absorption from the probing fluorescent nanosphere, we use fluorescent spheres with low absorption probability of $2 \times 10^{-4}\%$ [3]. The absorption probability is the ratio of the absorption cross section to the physical cross section of the fluorescent spheres. Moreover, the concentration of the fluorescent spheres in the samples is of the order of $10^{-5} \mu\text{m}^{-3}$, which results in an albedo $a \approx 1 - 10^{-8}$ [4]. Since single fluorescent nanospheres have an extremely low absorption probability and albedo, the ZnO scattering medium is lossless with well-defined transmission channels.

2. SETUP, ACQUISITION TIMES, AND NOISE

Our experimental setup is shown in Figure S1. A continuous wave (cw) excitation laser beam (Cobolt Jive, 100 mW, $\lambda_e = 561$ nm) is coupled to a single mode fiber (SMF) for spatial mode cleaning, and expanded to 8 mm beam diameter to illuminate a spatial light modulator (SLM, Holoeye PLUTO-VIS-014-C). The SLM controls the wavefront of the reflected light. Through an imaging configuration, a twice demagnified image of the

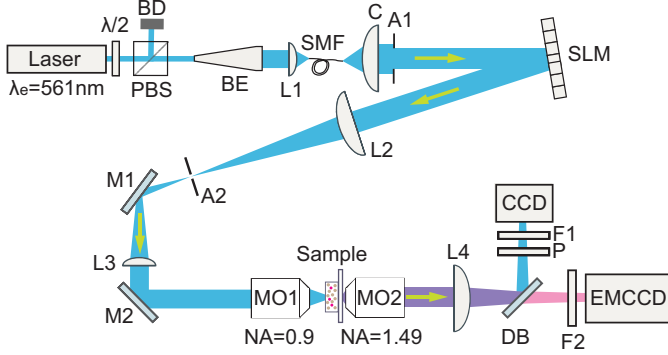


Fig. S1. Experimental setup: the cw laser beam ($\lambda_e = 561 \text{ nm}$) is spatially filtered and collimated to illuminate a phase-only reflection-type spatial light modulator (SLM) that controls the wavefront. The surface of the SLM is imaged to the entrance pupil of the first objective lens (MO1), and projected onto a scattering sample of ZnO nanoparticles doped with fluorescent spheres. The back surface of the sample is imaged onto an EMCCD camera to collect the fluorescent intensity and onto a CCD camera to collect the excitation light. $\lambda/2$ is a half-wave plate, PBS a polarizing beam splitter, BD a beam dump, BE a beam expander, SMF a single-mode fiber, L1, L2, L3, and L4 lenses with focal distances 11 mm, 200 mm, 100 mm, and 500 mm, respectively, C a collimator, A1 and A2 apertures, M1 and M2 mirrors, MO1 and MO2 microscope objectives, DB a dichroic beam splitter, F1 and F2 filters, and P is a polarizer.

SLM is formed at the entrance pupil of the first objective MO1 (Nikon: infinity corrected, $100\times$, $\text{NA} = 0.9$) to give a $0.31 \mu\text{m}$ focused spot with a planar wavefront and estimated to be about $56 \mu\text{m}$ with a random wavefront. The position of the scattering medium was controlled by a piezoelectric scanning stage. By using a microscopy configuration composed of an immersion oil objective MO2 (Nikon: Infinity corrected, $60\times$, $\text{NA} = 1.49$) and a tube lens L4 (focal length $f = 50 \text{ cm}$), the back surface of the sample is imaged onto a CCD camera (Allied Vision Technologies Stingray F-145) to detect the excitation light, and onto an electro-magnified camera (EMCCD, Andor iXon Ultra 897) to sensitively detect the weak fluorescent light. The excitation laser light and fluorescent light were separated by a dichroic beam splitter (DB) in the microscopy configuration.

We chose to limit the number of degrees of freedom on the SLM to $N = 900$, in order to optimize the fidelity versus the time it takes to do optimization experiments, notably since the required fluorescence measurements lead to unavoidable bleaching of the fluorescent nanospheres. We find that with $N = 900$ controlled pixels on the SLM, the optimization time is a feasible 20 minutes, while for $N = 3000$ pixels the optimization time already exceeds 1 hour. Due to the low number of degree of control on the SLM, we obtained a typical enhancement of about 270, which is sufficient for our experiment.

Let us briefly elaborate on the data acquisition times, as this ultimately limits the amount of data we could collect. Data such as the ones shown in Figure 5 in the main manuscript take about 20 minutes to collect. Data as in Figure 6 of the main manuscript take about 2 days per data point to collect, namely, $m_2 = 100$ scans times 20 minutes, plus additional time for alignment. All data as shown in Figure 3 take more than about 1 month to measure. The long acquisition times therefore limit the number of data points that can be collected, and prohibit to investigate

whether there are deviations from the cylindrical symmetry in the physical problem at hand.

For an extensive discussion on noise in a similar wavefront shaping, we refer to Ref. [5]. Based on that work, we conclude that the error bars on the fluorescence enhancement and on the fidelity are about 4% and 14%, respectively. We attribute the large variation of the fluorescent enhancement to the low signal-to-noise ratio due to the singly illuminated fluorescent particle. The maximum obtained fidelity depends notably on the ratio of the controlled segments to the number of channels in the sample, imperfections in phase modulation, temporal drifts, control of both polarizations, phase and amplitude control, and instability in environmental conditions. We limit the number of segments on the SLM on purpose to 900 to keep the measurement time reasonable. With 900 controlled segments (compared to 10^4 channels for the $16 \mu\text{m}$ -thick sample), the upper limit to the fidelity is $F \approx 0.1$.

3. MODELING THE THREE-DIMENSIONAL ENERGY DENSITY

The 3D energy density of light optimized to focus to a point by wavefront shaping is denoted $W_o(x, y, z)$. Following the maximal fluctuation principle described by Pendry *et al.* [6, 7], we approximate the transmission through fully open channels. This approximation implies that there are only ‘on’ and ‘off’ states, and that intermediate-transmission states are neglected. For a fully open channel we know from Ref. [5, 12] that the (x, y) -integrated energy density $W_o(z)$ is well described by only the fundamental diffusion eigenfunction²

$$W_o(z) = A W_{m=1}(z) = \int_{-\infty}^{\infty} \int_{-\infty}^{\infty} dx dy W_o(x, y, z), \quad (\text{S1})$$

where A is a proportionality constant. The fundamental diffusion eigenfunction that describes the energy density of an open channel is given by

$$W_{m=1}(z) = \frac{I_0 L_{\text{ex}}}{\pi D} \frac{\sin\left(\pi \frac{z+z_{e1}}{L_{\text{ex}}}\right)}{\cos\left(\pi \frac{z_{e2}}{L_{\text{ex}}}\right)}, \quad (\text{S2})$$

with I_0 the incident intensity, D the diffusion constant, and $L_{\text{ex}} = L + z_{e1} + z_{e2}$ [8], with z_{e1} and z_{e2} the extrapolation lengths of the front and back surfaces, respectively [2, 9].

Figure S2 illustrates that the optimized focus is taken to be the time reverse (or phase conjugate) of a perfectly focused beam that enters the sample from the back surface [10, 11]. The resulting ensemble-averaged energy density $W_{\text{dif}}(x, y, z)$ is described by the 3D diffusion equation in Fourier transformed transverse coordinates $(q_{\perp x}, q_{\perp y})$ as

$$W_{\text{dif}}(q_{\perp}; z, z_f) = \frac{P_{\text{in}}}{D} \frac{\sinh(q_{\perp} [L_{\text{ex}} - z - z_{e1}]) \sinh(q_{\perp} [z_f + z_{e1}])}{q_{\perp} \sinh(q_{\perp} L_{\text{ex}})} \quad (\text{S3})$$

where $q_{\perp} \equiv (q_{\perp x}^2 + q_{\perp y}^2)^{\frac{1}{2}}$ and P_{in} is the incident power. The solution in Eq. S3 only holds for $z > z_f$ (z_f the coordinate of a probing nanosphere), rather than z as used in the main manuscript

²The 1D fundamental diffusion eigenfunction has been applied to 3D samples and one of the main assumptions is that the 1D model considers translational invariance over an ensemble average. We thus conclude that a spatial ensemble average of the energy density corresponds to a (x, y) -integrated energy.

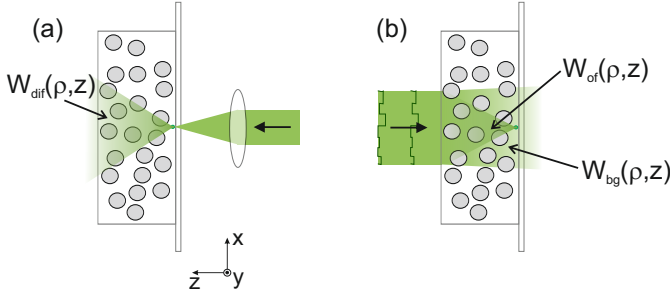


Fig. S2. Schematic illustration of the functions that describe optimized light in 3D inside a scattering medium. (a) A laser beam is focused at the back surface of the sample and the energy density $W_{\text{dif}}(x, y, z)$ of diffuse light is described using the diffusion equation. The focused beam is the time reverse of the component of optimized light that contributes to the optimized focus. (b) Optimized light propagating from left to right focuses light at the back surface of the sample. The energy density $W_o(x, y, z)$ of optimized light has two contributions: light that goes to the optimized focus $W_{\text{of}}(x, y, z)$ and the background $W_{\text{bg}}(x, y, z)$. The cartoon shows wavefront shaping in the absence of experiment imperfections, therefore $W_{\text{uc}} = 0$.

(for the full solution see Ref. [8]). We model the energy density of optimized light as a sum of two components

$$W_o(x, y, z) \equiv W_{\text{of}}(x, y, z) + W_{\text{bg}}(x, y, z). \quad (\text{S4})$$

where the functions $W_{\text{of}}(x, y, z)$ and $W_{\text{bg}}(x, y, z)$ are illustrated in Fig. S2. W_{of} is the energy density of light that propagates in a converging cone from the front surface to the back surface of the sample to obtain the optimized focus and W_{bg} is a background contribution due to incomplete time reversal of the focus, since the closed channels are not time-reversed. Due to imperfect wavefront shaping and experimental noise, W_e is observed in experiments and is related to W_o by Eq. 1 in the main manuscript that is repeated here:

$$W_e(x, y, z) = F.W_o(x, y, z) + (1 - F).W_{\text{uo}}(x, y, z). \quad (\text{S5})$$

W_{uc} describes uncontrolled light due to imperfect wavefront shaping and experimental noise and F is the fidelity. If we assume that the wavefront shaping experiment is perfect, *i.e.*, $F = 1$, the diffuse energy density vanishes: $W_{\text{uo}}(x, y, z; F = 1) = 0$ and $W_e = W_o$.

At first sight, one might naively think that the energy density W_{dif} is equal to W_{of} . This reasoning is not plausible, however, as W_{of} contains only open channels, therefore its z -dependent profile must track $W_{m=1}(z)$. Therefore, to obtain W_{of} , we normalize W_{dif} and map it onto the profile of $W_{m=1}(z)$:

$$W_{\text{of}}(x, y, z) = A_1 \frac{W_{\text{dif}}(x, y, z)}{\int_{-\infty}^{\infty} \int_{-\infty}^{\infty} dx dy W_{\text{dif}}(x, y, z)} W_{m=1}(z), \quad (\text{S6})$$

where A_1 is a normalizing amplitude factor. As the background term W_{bg} does not contribute to the optimized focus, and as we consider perfect shaping in the maximal fluctuation approximation, W_{bg} consists of only open channels. We describe the background term W_{bg} in (x, y) by mapping the z -dependent $W_{m=1}$ onto a Gaussian with constant width ρ_0 along z

$$W_{\text{bg}}(\rho, z) = \frac{A_2}{\pi\rho_0^2} W_{m=1}(z) \exp[-\rho^2/\rho_0^2], \quad (\text{S7})$$

with A_2 a normalizing constant of the background intensity, and $\rho \equiv (x, y)$. It is justified to take the Gaussian width to be constant throughout the medium, since the diffuse beam width (about $\rho_0 = 56 \mu\text{m}$) exceeds the sample thickness.

The constants $A_{1,2}$ are constrained such that the intensity pattern of the optimized light at the back surface is obtained. We determine A_1 from the fact that for perfect wavefront shaping ($F = 1$), the total intensity in the optimized focus is proportional to the total transmission ($T_{\text{tot}} \sim \ell/L$) before wavefront shaping, therefore $A_1 = T_{\text{tot}} I_0$. The intensity in the background A_2 is therefore the total transmitted intensity of an open channel ($T = 1$) minus the intensity in the focus: $A_2 = (1 - T_{\text{tot}}) I_0$. Since we are considering the maximum fluctuation approximation, we have considered the transmission of an open channel (equal to 1) rather than 2/3, resulting from the weighted transmission of all channels used in Ref. [5].

Similar as in Eq. (S7), we describe the 3D energy density of unoptimized light $W_{\text{uo}}(\rho, z)$ by mapping the z -dependent solution of the 1D diffusion equation $W_d(z)$ in (x, y) onto a Gaussian profile with a constant width ρ_0 along z

$$W_{\text{uo}}(\rho, z) = \frac{1}{\pi\rho_0^2} W_d(z) \exp[-\rho^2/\rho_0^2], \quad (\text{S8})$$

where $W_d(z)$ is given by

$$W_d(z) = \frac{I_0}{D} \left[\frac{z_{\text{inj}} + z_{e1}}{L_{\text{ex}}} (L + z_{e2} - z) - z_{\text{inj}} \exp(-\frac{z}{z_{\text{inj}}}) \right], \quad (\text{S9})$$

with z_{inj} the injection depth where incident light becomes diffuse, which accounts for the angular distribution of the incident shaped wavefront.

The procedure described above guarantees that the total stored energy in the 3D energy density $W_o(x, y, z)$ equals the one for open channels $W_{m=1}(z)$. To verify this balance, we calculated numerically the difference

$$\Delta = \frac{\int_{V_s} dV W_o(x, y, z)}{\int_{V_s} dV W_{\text{uo}}(x, y, z)} - \frac{\int_0^L dz W_{m=1}(z)}{\int_0^L dz W_d(z)} \quad (\text{S10})$$

where V_s is the sample volume, and $dV = dx dy dz$. While Δ is expected to be equal to 0, we obtain $\Delta = 1.2 \times 10^{-13}$ and $\Delta = 2 \times 10^{-13}$ for the sample with $L = 8 \mu\text{m}$ and $16 \mu\text{m}$, respectively. This accuracy confirms that our procedure is consistent.

It is a relevant question whether Eq. (1) of the main text (Eq. S5 above) is valid without ensemble averaging, in the sense of the traditional habit in the study of random media to average over speckle patterns by averaging over many different positions, see, *e.g.*, Ref. [13]. There are several reasons why the speckle is averaged out when we apply Eq. (1) to describe our experimental observations. Firstly, since our experiment is effectively a fluorescence study, there is no phase relation between the incident excitation speckle field and the fluorescence that we detect. Secondly, the number of excitation speckles within each fluorescent sphere is about $N = 10$. The fluorescence excited by each of these N speckle spots is mutually incoherent, so that the fluorescence signal is effectively averaged, to within about $1/N$ relative error, or about 10%, much less variation than would be observed with elastic scattered speckle. Thirdly, our experiments average over the incident wavefronts, that each corresponds to one volume speckle pattern inside each sample. Thus, we average over $m = 4100$ configurations per data point, sufficient to reliably determine an average differential fluorescence enhancement, as shown in Fig. 6 of the main text.

In our experiments, we measured the fluorescent intensity from single probe nanospheres that are located at a specific position z and transverse coordinates (x, y) inside the 3D scattering medium. We define the fluorescence enhancement η_f^p from a single nanosphere to be

$$\eta_f^p \equiv \frac{F_o(x, y, z)}{F_{uo}(x, y, z)}, \quad (\text{S11})$$

where the fluorescence energy fluxes F_o and F_{uo} are obtained from the optimized energy density W_o and the unoptimized energy density W_{uo} , respectively. We note here that η_f^p is the fluorescence enhancement at perfect fidelity $F = 1$ and is related to the differential fluorescent enhancement $\partial\eta_f/\partial F$ by

$$\eta_f^p = \frac{\partial\eta_f}{\partial F} + 1 \quad (\text{S12})$$

derived from Eq. S5. The flux of the optimized light is equal to

$$F_o(x, y, z) = \int_V dx' dy' dz' c W_o(x', y', z') \frac{z_f + z_{e1}}{DL_{ex}}, \quad (\text{S13})$$

where the volume integral accounts for the finite volume V of the probe particle, c is a proportionality constant that relates the power to the energy density. The factor $\frac{z_f + z_{e1}}{DL_{ex}}$ accounts for the diffusion the fluorescent emission from the nanosphere at z_f reaching the back surface of the sample $z = L$. Similarly, the flux due to unoptimized light is

$$F_{uo}(x_f, y_f, z_f) = \int_V dx' dy' dz' c W_{uo}(x', y', z') \frac{z_f + z_{e1}}{DL_{ex}}, \quad (\text{S14})$$

Substituting Eqs. S13 and S14 into Eq. S11, we obtain the position-dependent fluorescence enhancement η_f^p .

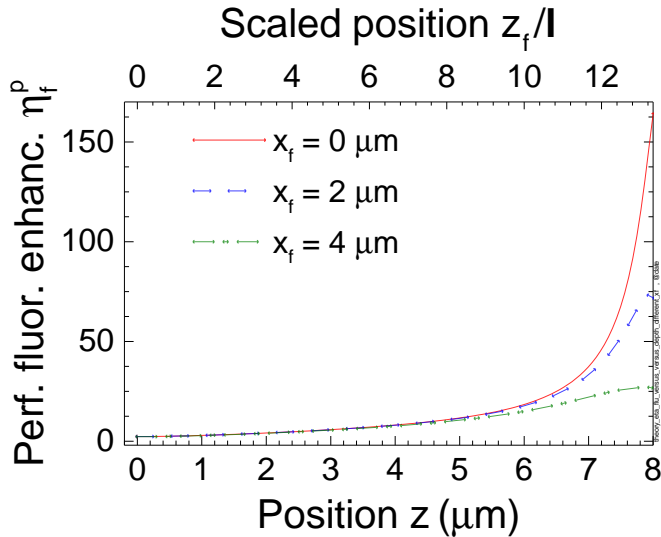


Fig. S3. Fluorescent enhancement η_f^p versus depth z from Eq. S11. The red solid, blue dash-dot, and green dash curves are for probe particle positions $(x_f, y_f) = (0, 0) \mu\text{m}$, $(2, 0) \mu\text{m}$, and $(4, 0) \mu\text{m}$, respectively. (The red solid curve is the same as in Fig. 2a of the main manuscript). Sample parameters are $L = 8 \mu\text{m}$, transport mean free path $\ell = 0.6 \mu\text{m}$, and the extrapolation lengths are $z_{e1} = 2.19\ell$, $z_{e2} = 0.68\ell$.

Figure S3 shows η_f^p as a function of depth z of the fluorescent particle using Eq. S11 for particles at different transverse coordinates x (equivalent to y coordinates). η_f^p increases from the front surface of the sample and peaks at the back surface for all x . The increase of η_f^p towards the back surface is due to the focusing of the wavefront shaped light. The enhancement η_f^p at the center of the illuminated area $x = 0 \mu\text{m}$ is about 2 to 4× greater than for probe particles displaced by $\Delta x = 2 \mu\text{m}$ and $4 \mu\text{m}$ from the center, respectively. This dependency of η_f^p on the transverse coordinate x shows that our model correctly captures the 3D distribution of the energy density.

REFERENCES

1. E.G. van Putten, *Disorder-enhanced imaging with spatially controlled light*, Ph.D. thesis (University of Twente, 2011) available from <https://www.complexphotonicssystems.com>.
2. J.X. Zhu, D.J. Pine, and D.A. Weitz, "Internal reflection of diffusive light in random media," *Phys. Rev. A* **44**, 3948 (1991).
3. G. van Soest, *Experiments on random lasers* Ph.D. thesis (Univ. Amsterdam, 2001), available from www.complexphotonicssystems.com
4. C.F. Bohren and D.R. Huffman, *Absorption and scattering of light by small particles* (Wiley, New York, 1983)
5. O.S. Ojambati, H. Yilmaz, A. Lagendijk, A.P. Mosk, and W.L. Vos, "Coupling of energy into the fundamental diffusion mode of a complex nanophotonic medium," *New J. Phys.* **18**, 043032 (2016).
6. J.B. Pendry, A. MacKinnon, and A.B. Pretre, "Maximal fluctuations – a new phenomenon in disordered systems," *Physica A* **168**, 400 (1990).
7. J.B. Pendry, A. MacKinnon, and P.J. Roberts, "Universality classes and fluctuations in disordered systems," *Proc. R. Soc. London, Ser. A* **437**, 67 (1992).
8. I.M. Vellekoop, E.G. van Putten, A. Lagendijk, and A.P. Mosk, "Demixing light paths inside disordered metamaterials," *Opt. Express* **16**, 67 (2008).
9. A. Lagendijk, R. Vreeker, and P. de Vries, "Influence of internal reflection on diffusive transport in strongly scattering media," *Phys. Lett. A* **136**, 81 (1989).
10. I.M. Vellekoop, "Feedback-based wavefront shaping," *Opt. Express* **23**, 12189 (2015).
11. I.M. Vellekoop and A.P. Mosk, "Universal Optical Transmission of Light Through Disordered Materials," *Phys. Rev. Lett.* **101**, 120601 (2008).
12. O.S. Ojambati, A.P. Mosk, I.M. Vellekoop, A. Lagendijk, and W.L. Vos, "Mapping the energy density of shaped waves in scattering media onto a complete set of diffusion modes," *Opt. Express* **24**, 18525 (2016).
13. M.P. van Albada and A. Lagendijk, "Observation of weak localization of light in a random medium," *Phys. Rev. Lett.* **55**, 2692 (1985); P.E. Wolf and G. Maret, "Weak localization and coherent backscattering of photons in disordered media," *Ibid.* **55** 2696 (1985).
14. D. Akbulut, T. Strudley, J. Bertolotti, A. Lagendijk, O.L. Muskens, W.L. Vos, and A.P. Mosk, "Optical transmission matrix as a probe of the photonic strength," *Phys. Rev. A* **94**, 043817 (2016).